Acta Orthopaedica et Traumatologica Turcica 53 (2019) 239–247

Contents lists available at ScienceDirect

Acta Orthopaedica et Traumatologica Turcica

journal homepage: https://www.elsevier.com/locate/aott

Correlation of 3-T MRI and CT findings with patient symptoms and treatment outcome in radiofrequency ablation of osteoid osteoma

Mehmet Ali Kaptan [a, *], Berat Acu [a], Çiğdem Öztunalı [b], Cüneyt Çalışır [a], Ulukan İnan [c], Muzaffer Bilgin [d]

[a] Osmangazi University Faculty of Medicine, Department of Radiology, Eskisehir, Turkey
[b] Gazi University Faculty of Medicine, Department of Radiology, Ankara, Turkey
[c] Osmangazi University Faculty of Medicine, Department of Orthopaedics and Traumatology, Eskisehir, Turkey
[d] Osmangazi University Faculty of Medicine, Department of Biostatistics, Eskisehir, Turkey

ARTICLE INFO

Article history:
Received 5 February 2017
Received in revised form
13 January 2019
Accepted 28 April 2019
Available online 16 May 2019

Keywords:
Ablation
CT
MRI
Osteoid osteoma
Radiofrequency

ABSTRACT

Objective: The aim of this prospective study was to evaluate pre- and post-treatment MRI and CT findings of osteoid osteoma (OO) patients treated with radiofrequency thermo-ablation (RFTA) and to compare these findings with visual analog scale (VAS) scores.
Methods: Sixteen patients (4 females and 12 males; mean age of 18.87 ± 8.75 years (range: 8–37)) with OO were examined with CT and MRI, at baseline and at an average of 3 months following the procedure. On pre- and post-procedural CT and MRIs, OO-related findings were recorded. Treatment success was evaluated with VAS scores.
Results: Baseline VAS scores were 8 or 9 and follow-up scores were 0 or 1, indicating no early recurrences.
Nidus diameters decreased significantly after the procedure ($p = 0.027$, $p = 0.002$, and $p = 0.002$; and $p = 0.001$, $p = 0.001$, $p = 0.001$ for AP, ML and CC nidus diameters for CT and MRI, respectively).
The mean nidus volume were significantly decreased after the procedure ($p = 0.001$, for CT and MRI).
On post-procedural images, cortical thickening, the signal intensity and contrast enhancement of the nidus and the extent of periostitis were significantly decreased ($p = 0.019$, $p = 0.001$, $p = 0.001$ and $p = 0.034$, respectively). There was no significant change in nidus calcification, perinidal cortical and intramedullary sclerosis, periosteal reaction, bone deformity, bone marrow and soft tissue edema, joint effusion and synovitis after the procedure ($p = 0.253$, $p = 0.062$, $p = 0.245$, $p = 1$, $p = 1$, $p = 0.429$, $p = 0.371$, $p = 0.625$, $p = 1$).
Conclusion: Although the changes in imaging findings may be helpful in early follow-up of OO patients treated with RFTA, these changes alone cannot be used with accuracy in predicting treatment response.
Level of Evidence: Level IV, Therapeutic Study.

Introduction

Osteoid osteoma (OO) is a benign, osteoblastic tumor that is characterized by a small central nidus and peripheral reactive bone formation. It mostly occurs in patients between the ages of 7–25.[1] OO is mostly found at the metaphyseal–diaphyseal junction of the long bones.[2,3] In more than 50% of cases, OO occurs in femur and tibia.[1,4]

Current treatment options for OO are conservative treatment with non-steroidal anti-inflammatory drugs (NSAIDs), surgical resection and percutaneous local ablative treatments. Imaging-guided percutaneous ablation techniques include alcohol ablation, interstitial laser ablation (ILA), high intensity focused ultrasound (HIFU) ablation, cryoablation and radiofrequency thermal ablation (RFTA).[5] Currently, radiofrequency thermo-ablation of OO

* Corresponding author. Osmangazi University Faculty of Medicine, Department of Radiology, Eskisehir, 26040, Turkey. Tel.: +90 222 239 29 79; fax: +90 222 239 37 72.
E-mail address: mealikaptan@gmail.com (M.A. Kaptan).
Peer review under responsibility of Turkish Association of Orthopaedics and Traumatology.

https://doi.org/10.1016/j.aott.2019.04.015

is one of the most widely accepted methods in treatment. Although the pre-procedural imaging findings of OO are well-known, few studies evaluated the post-procedural changes in imaging findings of OO. Recent studies suggested that these changes in post-procedural imaging findings might be used in evaluation of the treatment success after RFTA.[6]

In this study, we aimed to assess the effectiveness of RFTA, by analyzing the relationship between the pre- and post-procedural CT and MRI findings and the visual analog scale (VAS) scores of osteoid osteoma patients treated with RFTA.

Materials and methods

The approval of the ethics board for non-pharmacological clinical trials was obtained. Sixteen consecutive patients treated with CT-guided RFTA between August 2014 and May 2016 were involved in the retrospective study. Non-enhanced CT and contrast-enhanced MRI were performed before and after RFTA treatment. No percutaneous biopsies were performed before the procedures. The diagnosis of OO was made if the presence of the nidus had been confirmed in CT studies and if the patient had the clinical findings of OO. Clinical findings included a chronic (more than six months), non-mechanical pain, which worsens at night and responds well to NSAIDs. A history or presence of a primary malignancy or metastatic disease was an exclusion criterion. For clinical evaluation, all patients were asked to fill out VAS questionnaires before and after the procedure. Written informed consent was obtained from all patients. Pregnancy, local infection in the procedure area, systemic infection or sepsis, and uncorrectable coagulopathy were accepted as contraindications for RFTA treatment; although none of the patients had any contraindications. The mean imaging follow-up period was 133.68 ± 138.29 days (range; 62–633 days, median; 97.5 days). The mean clinical follow-up period was 533.8 ± 298.01 days (range; 145–1170 days).

Patient population demographic characteristics

The age of the patients ranged between 8 and 37 years and the mean age was 18.87 ± 8.75. There were 4 female (25%) and 12 male (75%) patients. Ten OOs were located in the femur (62.5%), one was located in scapula (6.3%), one was located in humerus (6.3%), one was located in phalanx (6.3%), two lesions were located in tibia (% 12.5), and one lesion was located in radius (6.3%). Of the 16 lesions, six were located in the metaphysis (37.5%), nine lesions were located in diaphysis (56.3%) and one lesion was located at epiphysiometaphyseal junction. Thirteen lesions had an intracortical location (81.3%) and three of them were located in the subcortical medullary region (18.8%).

The demographic data are shown in Table 1.

CT protocol and measurements

Pre- and post-procedural CT examinations were performed on a 64-detector CT scanner (Aquillion 64; Toshiba Medical Systems Corporation, Otawara, Japan). The images were reconstructed with a section thickness of 0.5 mm, using a bone reconstruction kernel. For the manual measurements, the nidus volume was calculated from the anterior–posterior × medio-lateral × craniocaudal dimensions ×0,52 formula, using multiplanar CT images. For the software-aided CT measurements, images were evaluated at a workstation (GE Medical Systems AW volume share 5, Milwaukee, WI) and volume-rendered images were used in CT volume calculations. With the use of auto counter tool, manual adjustments were performed in order to obtain the optimal semi-automated nidal volume calculations.

MRI protocol and measurements

Pre- and post-procedural examinations were performed with a 3-T MRI device (General Electric Healthcare, Milwaukee, WI, USA), using a sixteen-channel flexible coil (GEM suite, GE Healthcare, USA). Each examination included axial T1-weighted and STIR; axial and sagittal T2-weighted; axial fat-suppressed T2-weighted and fat suppressed PD; sagittal fat-suppressed PD, T1-weighted CUBE; coronal T1 weighted and T2-weighted, STIR and fat-suppressed PD; and post-contrast axial T1-weighted and sagittal T1-weighted CUBE images. For the manual measurements, the nidus volume was calculated from the anterior–posterior × medio-lateral × craniocaudal dimensions ×0,52 formula, using T1-weighted MR images. For the software-aided MRI measurements, the images were evaluated at a workstation (GE Medical Systems AW volume share 5, Milwaukee, WI). T1 weighted FSE CUBE sequences with 3D MIPs were used in MRI volume calculations. With the use of auto counter tool, manual adjustments were performed in order to obtain the optimal semi-automated nidal volume calculations.

RFTA protocol

Prior to procedure, a complete blood count was performed and biochemical and blood coagulation parameters were

Table 1
Patient population demographic results.

Patient number	Gender	Age	Bone location	Pre-procedure VAS Average	Post- procedure VAS Average	Complication
1	Female	29	Femur	8	0	None
2	Male	37	Tibia	8	1	Focal osteomyelitis
3	Male	24	Femur	8	0	None
4	Male	8	Femur	8	0	None
5	Male	25	Femur	9	0	None
6	Male	11	Femur	9	0	None
7	Male	20	Radius	9	0	Soft tissue-subcutaneous edema
8	Male	19	Scapula	9	0	None
9	Male	16	Humerus	9	0	None
10	Male	17	Phalanx	9	0	Skin burn
11	Female	9	Femur	8	0	None
12	Male	25	Femur	8	0	None
13	Male	10	Femur	9	0	None
14	Female	11	Femur	9	0	None
15	Female	11	Tibia	9	0	Soft tissue-subcutaneous edema
16	Male	30	Femur	9	0	None

VAS: visual analog scale.

evaluated. A prophylactic antibiotic agent was injected intravenously. All procedures were performed in the CT suite. Anesthesia procedures for RF ablations were performed by a dedicated anesthesia team with the use of sedoanalgesia (with administration of ketamine, propofol, midazolam or fentanyl in proper dosages) and close monitoring of oxygen saturation and cardiorespiratory functions. After precise localization of the lesion with CT, the skin entry point was determined. A small incision was made at the skin entry point and a 13-gauge 10–15 cm bone biopsy needle was used to reach the nidus. For RF ablations, a bipolar 17-gauge cooled-tip probe with a 2-cm active tip (VIVA RF® system RFTA electrodes STARmedCo. Ltd. GYEONGGI-DO, KOREA or CoATHERM RF® system RFTA electrodes Apro Korea Inc. GYEONGGI-DO, KOREA) was inserted into the nidus and was connected to the RF generator. Energy application was started at 60 W and was gradually increased 10 W per minute, up to a maximum of 100 W. Once a maximum of 100 W was reached, 100 W was used during the rest of the ablation time. The procedure was terminated if a resistance of 800 Ω was reached.

Post-procedural clinical and radiological assessment and follow up

The patients in the study experienced early post-procedural pain which was managed with administration of IV paracetamol, or narcotic analgesics (tramadol) when necessary, under close monitoring in hospital settings. Patients were hospitalized and kept under close observation in orthopedics department for one day. Patients were clinically assessed one day after the procedure and discharged if no problems were observed. For the first month after the procedure, avoiding active sports and heavy exercises was recommended.

All patients were clinically assessed at 1st week, 1st month and 3rd month. During the first two of these follow-up visits, the skin entry site was evaluated and the clinical regression was questioned. During the third follow-up visit, patients were asked to fill out VAS questionnaires and non-enhanced CT and contrast-enhanced MRI were obtained.

Evaluation of CT, MRI and visual analog scale (VAS) findings

Pre- and post-procedural CT and contrast-enhanced MRI were evaluated at a GE Medical Systems AW volume share 5 workstation (General Electric Healthcare, Milwaukee, WI). All images were evaluated in consensus by two radiologists with 16 and 4 years of experience. Evaluated imaging findings are shown in Table 2.

Statistical analyses

Non-parametric testing was used for statistical analyses. Wilcoxon's signed rank test, McNemar's test and marginal homogeneity test were used for comparison of dependent groups and Kruskal–Wallis and Mann–Whitney U tests were used for comparison of independent groups. Statistical analyses were performed using SPSS software (IBM Corp. Released 2012. IBM SPSS Statistics for Windows, Version 21.0. Armonk, NY: IBM Corp.), and the statistical significance was set at $p < 0.05$.

Results

CT and MRI results

CT and MRI measurements of nidus dimensions

On CT, pre- and post-procedural average nidus diameters were significantly different ($p = 0.027$, $p = 0.002$, and $p = 0.002$ for AP, ML and CC diameters, respectively).

On MRI, pre- and post-procedural average nidus diameters were significantly different ($p = 0.001$, $p = 0.001$ and $p = 0.001$ for AP, ML and CC diameters, respectively) (Table 3).

CT and MRI measurements of nidus volume

For both CT volume measurement methods, pre- and post-procedural average nidus volumes were significantly different ($p = 0.001$, $p = 0.001$ for manual and semi-automated measurements, respectively).

Table 2
CT-MRI evaluation criteria.

CT evaluation criteria	MRI evaluation criteria
AP, ML, CC diameters before and after the procedure	AP, ML, CC diameters before and after the procedure
Manually calculated volume before and after the procedure (AP × ML × CC × 0.52)	Manually calculated volume before and after the procedure (AP × ML × CC × 0,52)
Automatically calculated volume before and after the procedure (3D volume created with “post-processing” in workstation)	Automatically calculated volume before and after the treatment (3D volume created with "post-processing" in workstation)
Nidus calcification, before and after the procedure	Nidus intensity before and after the procedure (T1, T2, PD, STIR)
Presence or absence of cortical thickening, before and after the procedure	Presence or absence of bone marrow and/or soft tissue edema, before and after the procedure
Thickness of the cortex at the level of the nidus on pre- and post- procedural axial images, if cortical thickening is present	Largest width of the edema area on pre- and post-procedural sagittal images, if bone marrow edema is present
Thickness of the cortex at the level of the nidus on pre- and post- procedural axial images, if cortical thickening is present	Periostitis, before and after the procedure
Presence or absence of bone deformity, before and after the procedure	Distance between the nidus and the nearest joint, presence or absence of joint effusion and/or synovitis, before and after the procedure
Perinidal cortical and/orintramedullary sclerosis, before and after the procedure	Presence or absence of muscle atrophy, before and after the procedure
Periosteal reaction, before and after the procedure	Post-contrast nidus SI and nidus contrast enhancement ratio, before and after the procedure
Evaluation of visual analog system changes	
The average VAS pain score, before the procedure	
What treatment(s) was/were received before the procedure – how much pain relief was achieved with this/these treatments	
The average VAS pain score, after the procedure	
How much the need for pain medication was reduced after the procedure	
How much benefit did RFTA treatment provided	

AP: anteroposterior, CC: craniocaudal, ML: mediolateral, RFTA: radiofrequency thermoablation, SI: signal intensity, VAS: visual analog scale.

Table 3
CT and MRI measurements of nidus dimensions and nidus volume.

CT measurements of nidus diameters				MRI measurements of nidus diameters			
Nidus diameter (mm ± SD)	**Pre-procedure**	**Post-procedure**	***p***	**Nidus diameter (mm)**	**Pre-procedure**	**Post- procedure**	***p***
AP	6.43 ± 2,18	5.06 ± 2,62	0,027	AP	6.52 ± 2,68	4,63 ± 2,34	0,001
ML	6,46 ± 1,88	5.45 ± 1,94	0,002	ML	6,15 ± 1,9	4,69 ± 2,14	0,001
CC	11,81 ± 4,29	9,65 ± 3,51	0,002	CC	10,45 ± 3,67	7,46 ± 3,78	0,001
Nidus volume (mm^3)	**Pre-procedure**	**Post-procedure**	***p***	**Nidus volume (mm^3)**	**Pre-procedure**	**Post-procedure**	***p***
Manual	317,05 ± 189,73	205,51 ± 161,05	0,001	Manual	291,03 ± 210,99	154,93 ± 161,33	0,001
Semi-automated	375,25 ± 234,13	230,5 ± 185,57	0,001	Semi-automated	354,25 ± 226,77	192,93 ± 172,36	0,001

AP: anteroposterior, CC: craniocaudal, ML: mediolateral.

For both MRI measurement methods, pre- and post-procedural average nidus volumes were significantly different ($p = 0.001$, $p = 0.001$ for manual and semi-automated measurements, respectively) (Table 3). The differences between the manual and semi-automated volume measurements were statistically significant ($p = 0.001$, both pre- and post-procedurally). In all patients, semi-automated CT and MRI measurements resulted in higher values than the manual measurements.

In one patient (patient no 7), the evaluation of post-procedural CT and MRI revealed an increase in nidus size and volume. This increase was evident on both manual and semi-automated CT and MRI measurements. In another patient (patient no 1), 3rd month follow-up CT and MRI examinations were not available because the patient was planning a pregnancy during that time. She had her follow-up CT and MR examinations 633 days after the procedure. On follow-up images, the nidus was barely visible on CT and it was indistinguishable from the surrounding cortical bone on MRI.

Nidus calcification

According to the extent of calcification as a percentage of the cross-sectional area of the nidus, the nidus calcification was classified into one of four groups, (≤25%, 26–50%, 51–75%, and ≥76%). With regard to the presence/absence or the extent of the nidus calcification, no statistically significant difference was found between the pre- and post-procedural CT examinations, ($p = 0.253$).

Cortical thickening

The presence or absence of cortical thickening was evaluated on CT. In cases that demonstrated reactive cortical thickening, the thickness of the cortex was measured at the level of the nidus on axial and sagittal images. On axial and sagittal images, the average pre-procedural cortical thicknesses were 7,37 ± 4,36 mm and 33,45 ± 26,62, respectively. The average post-procedural cortical thicknesses were 5,91 ± 3,51 mm and 27,85 ± 26,01 mm on axial and sagittal images, respectively. A significant difference was found between the pre- and post-procedural measurements of cortical thickening ($p = 0.019$ and $p = 0.019$, for axial and sagittal plane measurements, respectively).

Perinidal cortical and intramedullary sclerosis

According to the extent of sclerosis on CT, the cortical or intramedullary sclerosis was visually classified into one of four groups, as; none, mild, moderate, and severe. No statistically significant difference was found between the pre- and post-procedural examinations ($p = 0.062$, $p = 0.245$).

Periosteal reaction

On CT, the periosteal reaction was evaluated at the level of the nidus and was visually classified into one of four groups, as; none, mild, moderate and severe. No statistically significant difference was found between the pre- and post-procedural CT examinations ($p = 1$).

Bone deformity

The presence or absence of bone deformity was evaluated on CT and no statistically significant difference was found between pre- and post-procedural examinations ($p = 1$).

Nidus signal intensity changes

On pre- and post-procedural MRIs, the signal intensity of the nidus was evaluated on T1-weighted, T2-weighted, PD, and STIR sequences. In all series, the signal intensity of the nidus was visually compared to that of the normal muscle and was classified into one of four groups: group 1, homogeneously hyperintense; group 2, homogeneously hypointense; group 3 homogeneously isointense; and group 4 heterogeneous with hypo- and hyperintense areas. In the first 3 of these 4 groups, the signal intensity of the nidus was further subdivided into three categories as mild, moderate and severe.

On T1-and T2-weighted images, the differences between pre- and post-procedural nidus signal intensities were statistically significant ($p = 0.001$, $p = 0.001$ for T1-and T2-weighted images, respectively). With regard to nidus signal intensity, STIR and fat-suppressed PD images were significantly correlated with each other and the differences between pre- and post-procedural nidus signal intensities were also statistically significant on these sequences ($p = 0.001$, $p = 0.001$, for fat-suppressed PD and STIR images, respectively) (Figs. 1 and 2a–d).

Bone marrow and soft tissue edema

On fat suppressed T2-weighted images, bone marrow edema was visually graded as none, mild, moderate and severe. When present, the extent of the edema was evaluated by measuring the width of the edema zone at its largest diameter on sagittal images. With regard to presence or absence of bone marrow edema, no statistically significant difference was found between the pre-and post-procedural images ($p = 0.429$). Also, the extent and the severity of the edema were not significantly different on pre- and post-procedural images ($p = 041$ and $p = 0.371$, respectively). Soft tissue and/or muscle edema was visually graded as none, mild, moderate or severe, and no statistically significant difference was found between the pre-and post-procedural images ($p = 0.371$).

Periostitis

The presence or absence of periostitis was evaluated on pre- and post-procedural contrast-enhanced T1-weighted images and T2-weighted images, at the level of the nidus. The presence of periosteal contrast enhancement and circumferential high signal intensity on T2-weighted images were accepted to be positive for periostitis. Evaluation of pre- and post-procedural MRIs showed a

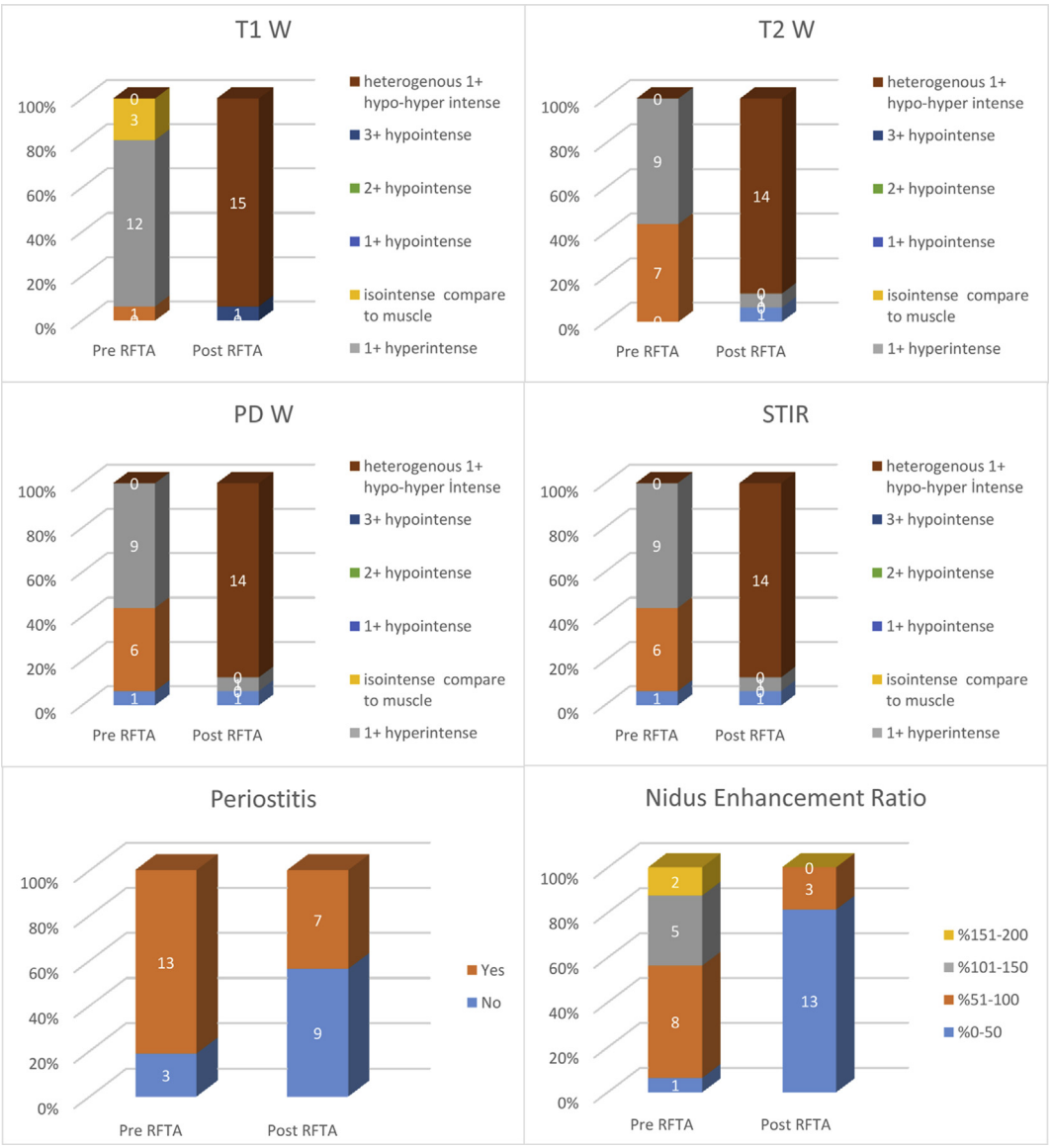

Fig. 1. Diagrams show pre- and post-procedural MRI signal intensities, periostitis and nidus enhancement ratio.

statistically significant difference in periostitis findings ($p = 0.034$) (Fig. 1).

Joint effusion and synovitis

In evaluation of pre- and post-procedural MRIs, the distance between the nidus and the nearest joint was measured. Presence or absence of joint effusion and/or synovitis was recorded. No statistically significant difference was found between the pre- and post-procedural examinations with regard to presence or absence of joint effusion and synovitis ($p = 0.625$ and $p = 1$ for effusion and synovitis, respectively). The nearest joint to nidus was hip joint in seven cases (43.8%), knee joint in five cases (31.3%), shoulder joint in two cases (12.5%), intermetacarpal joint in one case (6.3%), and distal interphalangeal joint in one case (6.3%). The mean distance between the nidus and the nearest joint was 68,37 ± 50,90 mm and a negative correlation was found between the nidus-joint distance and the presence of effusion and synovitis ($p = 0.013$ and $p = 0.02$, for effusion and synovitis, respectively).

Muscle atrophy

Muscle atrophy was evaluated with physical examinations and MR images. Three patients (23.07%) demonstrated clinical and imaging findings of muscle atrophy before the procedure. In these 3 patients, the findings were almost completely regressed at 3rd month follow-up. However, this change didn't reach a statistical significance ($p = 0.25$).

Nidus contrast enhancement

Contrast enhancement of the nidus was evaluated on contrast-enhanced T1-weighted MR images. For each patient, differences in signal intensities (SIs) of the nidus between pre- and post-contrast images (SI ratio of the nidus) were evaluated by region-of-interest (ROI) measurements on pre- and post-procedural scans. Also for each lesion, pre- and post-procedural contrast enhancement ratios were calculated using the following formula:

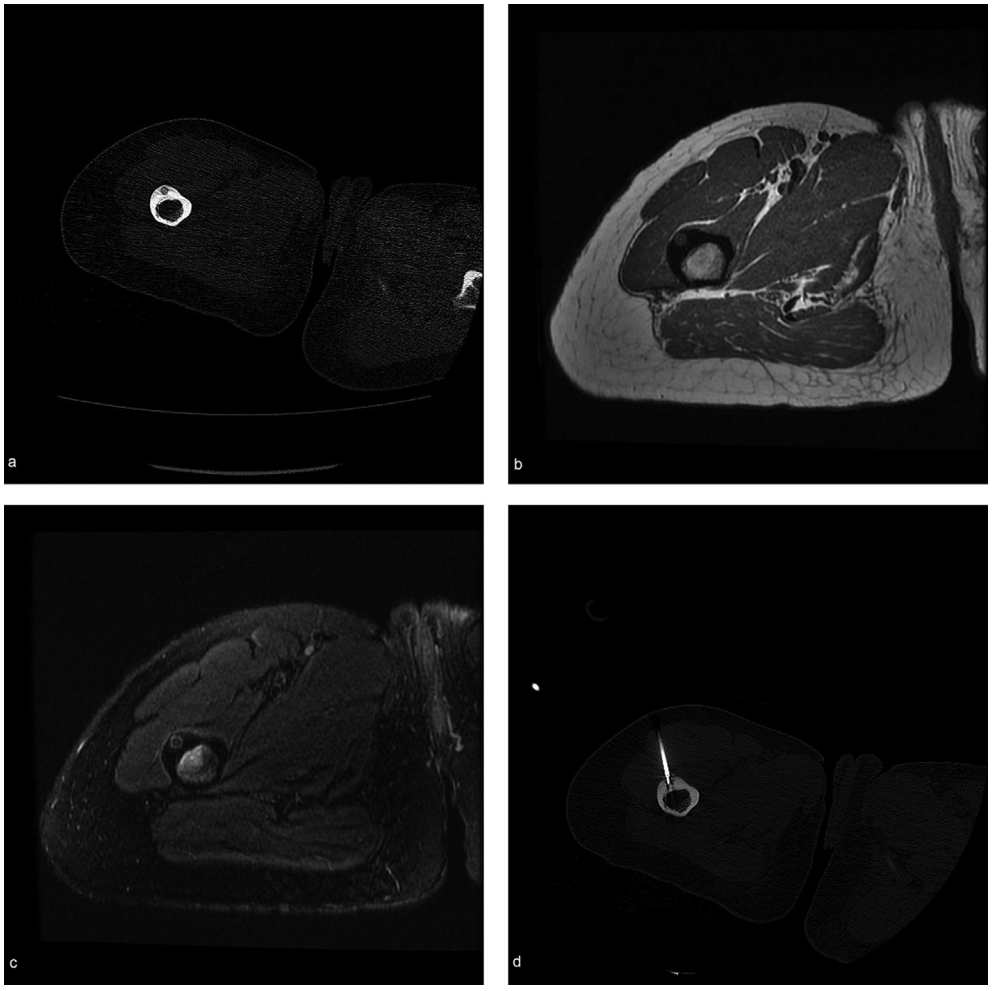

Fig. 2. Axial CT image (a) shows an intracortically located nidus with a central focus of calcification. Axial T1-weighted MR image (b) shows the signal intensity of nidus which is hyperintense when compared to that of the muscle. Axial fat-suppressed T2 – weighted MR image (c) shows the hyperintense nidus with a central isointense focus. Axial CT image (d) shows the radiofrequency electrode located centrally within the nidus.

$$\text{Contrast} - \text{enhancement ratio} = \frac{\text{Post contrast SI} - \text{Unenhanced SI}}{\text{Unenhanced SI} \times 100}$$

According to their contrast-enhancement ratios, the lesions were classified into four groups: group 1, contrast enhancement ratio between 0 and 50%; group 2, contrast enhancement ratio between 51 and 100%, group 3, contrast enhancement ratio between 101 and 150%; and group 4, contrast enhancement ratio between 151 and 200%.

The average pre- and post-procedural SI ratios were 2.5 ± 0.81 and 1.18 ± 0.4 ($p = 0.001$). Also, a significant difference was found between the pre- and post-procedural contrast enhancement ratios ($p = 0.001$) (Fig. 1).

MRI pattern after the procedure

Lee at al. evaluated post-procedural MRIs of the patients treated with RFTA and described a pattern of signal intensity changes in the treated areas. According to their description, contrast-enhanced T1-weighted and T2-weighted images demonstrate 3 different zones after RFTA treatment: an inner non-enhanced hypointense zone (Z1), a well-enhancing, hyperintense rim (Z2) and a peripheral, less hyperintense zone of background tissue (Z3).[6] In 11 out of 16 patients in our study (68.8%), this pattern of signal intensity changes was observed. In five patients (31.3%), the indicated pattern was absent. We didn't find a correlation between the presence of the described MRI pattern and the VAS scores ($p = 1$), and no correlation was found between the timing of the post-procedural follow up MRI and the presence of the described MRI pattern ($p = 0.661$) (Fig. 3a–c).

Clinical results

The patients quantified their pain on a VAS questionnaire, from 0 (no pain) to 10 (worst pain). Prior to procedure, all patients were using NSAIDs for pain relief and the VAS scores ranged between 8 and 9. After the procedure, relief of pain through the use of NSAIDs was also scored on a scale of 0% (no relief) to 100% (complete relief). Four patients at a rate of 80%, and twelve patients at a rate of 90%

reported benefiting from the treatment. Of the 16 patients, 15 reported no pain after the procedure (VAS score 0) and 1 patient reported a VAS pain score of 1.

Complications

Of the 16 patients, 4 had complications after the procedure. These were focal osteomyelitis (n = 1), edema of skin and subcutaneous tissues (n = 1), and thermal skin injury (n = 2).

Evaluation of success

The success of the treatment was evaluated in two categories: therapeutic success and technical success. Therapeutic success was defined as significant reduction in pain after treatment. According to analysis of the VAS scores, therapeutic success was achieved in 16 patients (100%). Technical success was defined as accurate insertion of RFTA electrode into the center of the nidus. For all patients in this study, CT scans obtained during the procedure confirmed that the RFTA electrode was located in the central nidus, therefore, a complete technical success (100%) was achieved.

Discussion

RFTA is one of the widely accepted local ablative techniques used in treatment of OO.[5] Although the reported technical success rates of RFTA range between 90 and 100%,[7] a residual tumor or symptomatic recurrences may occur after treatment. There is no consensus on the objective criteria that can be used in evaluation of treatment success or failure. The absence of objective imaging criteria for detection of recurrent or residual tumors may delay the diagnosis and retreatment of the patients. Depending on the location of the tumor, delayed diagnosis of these recurrent or residual tumors may result in severe complications such as osteonecrosis and degenerative discopathy.[8]

In dynamic contrast-enhanced studies, the majority of OOs demonstrate early contrast enhancement with an apparent contrast wash-out.[9] Successfully treated tumors are expected to exhibit different contrast-enhancement patterns. In our study, the pre- and post-procedural nidus contrast enhancement ratios and average SI ratios were significantly different ($p = 0.001$ and $p = 0.001$ for SI and contrast enhancement ratios, respectively).

The differences in pre- and post-procedural nidus dimensions were also statistically significant in our study. On CT, AP, ML and CC diameters of the nidus were significantly decreased after the procedure ($p = 0.027$, $p = 0.002$, and $p = 0.002$ for AP, ML and CC diameters, respectively). Similarly, on MR images, post-procedural AP, ML and CC diameters of the nidus were significantly decreased ($p = 0.001$; $p = 0.001$; $p = 0.001$ respectively). This change in nidus size on CT and MR studies is considered to be indicative of a successful nidus ablation and our findings are in accordance with the previous studies that reported a decrease in nidus size after RFTA treatment.[10]

However, in one patient in our study (patient no 7), the size of the nidus was found to be mildly increased after the procedure. This

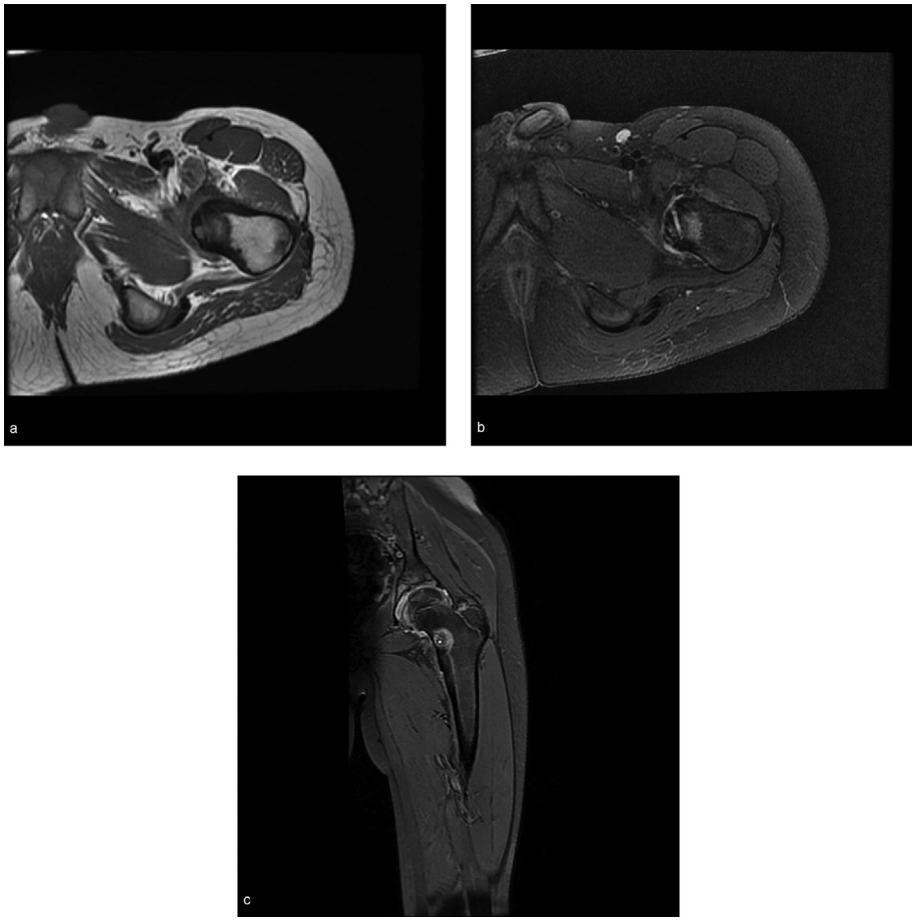

Fig. 3. Post-procedural axial T1-weighted MR image (a) demonstrates three different signal intensity zones at the level of the treated nidus. Post-procedural axial fat-suppressed PD MR image (b) shows the hyperintense cannula tract and perilesional increased signal intensity changes. Post-procedural coronal fat-suppressed PD MR image (c) shows hyperintense cannula tract and surrounding hypo- and hyperintense signal intensity zones. Also, note the increased signal intensity changes of the hip joint, consistent with synovitis.

increase in size was evident in all measured axes on CT and MR. MR images of the patient also demonstrated extensive edema of the bone marrow and soft tissues. On the other hand, the post-procedural signal intensity of the nidus was significantly decreased and the patient's post-procedural VAS score was 0. The post-procedural increase in nidus size in this patient was therefore accepted to be associated with the post-procedural reactive changes. The findings of the patient suggest that the post-procedural CT and MR measurements of the nidus size and/or volume do not always reflect treatment response or failure, particularly in cases that demonstrate extensive post-procedural edema of the bone marrow and soft tissues.

In evaluation of nidus volume, a statistically significant difference was found between the pre- and post-procedural CT and MRI measurements. The decrease in nidus volume was evident on both manual and semi-automated measurements.

In single axis measurements of the nidus diameter, post-procedural decrease in nidus diameter was found to be minimal or none in some of the patients. This was particularly true for single axis CT measurements. In single axis measurements of the nidus diameter, the post-procedural decrease in nidus diameter was more distinct in MRI than CT measurements. Therefore, we believe that MRI measurements would be preferable to CT measurements when evaluating a single axis of the nidus. Also, the volume measurements, rather than the single axis measurements would provide more accurate estimations of changes in nidus size. With regard to manual and semi-automated volume measurements of CT and MRI, we found a significant difference between the two volume measurement methods. We think that the difference between these two measurement methods may be related to asymmetry of the nidus. Therefore, semi-automated volume measurements using MRI sequences would give more accurate estimations of the volume.

Previous studies evaluating the treatment success of RFTA found that complete calcification of the nidus on follow-up CT studies was associated with successful treatment.[10,11] With regard to nidus calcification, we didn't find a statistically significant difference between the pre- and post-procedural CT examinations ($p = 0.253$). This was probably due to our shorter CT follow-up period, since the extensive calcified changes in nidus are reported to occur after twelve months on CT.[10,11]

In terms of presence or absence of cortical thickening, we didn't find a statistically significant difference between pre- and post-procedural examinations ($p = 1$) However, when present, a significant difference was found between the pre- and post-procedural measurements of cortical thickening ($p = 0.019$ and $p = 0.019$, for axial and sagittal plane measurements, respectively). This decrease in cortical thickening may be more pronounced on long-term follow up CTs.

With regard to cortical and/or intramedullary sclerosis and periosteal reaction, we found no statistically significant difference between the pre- and post-procedural CTs ($p = 0.062$, $p = 0.245$ and $p = 1$ for cortical sclerosis, intramedullary sclerosis, and periosteal reaction, respectively). We, therefore, think that CT follow-up studies may not demonstrate the decrease in reactive bone sclerosis and periosteal changes in early follow up period.

Pre- and post-procedural differences in signal intensities of the nidi were statistically significant in our study. In all series, the signal intensity of the nidus was significantly decreased after RFTA treatment ($p = 0.001$ for T1-weighted, T2-weighted, fat-suppressed PD and STIR images). These results are in accordance with the results published by Rehnitz et al, who found a significant decrease in the signal intensity of the nidus on T1-and T2-weighted images after RFTA treatment.[12] In our study, the post-procedural decrease in signal intensity of the nidus was more pronounced on T2-weighted, fat-suppressed PD and STIR images. Considering that the pre-procedural hyperintensity of nidus is reported to be associated with increased cyclooxygenase 1 (COX-1) and cyclooxygenase 2 (COX-2) levels, a post-procedural decrease in signal intensity of the nidus on T2-weighted images may also be associated with decreased pain after the treatment.[13] Therefore, a post-procedural decrease in signal intensity of the nidus on T2-weighted, fat-suppressed PD and STIR images may be used as an important finding when evaluating treatment response. Statistical results of our study support this hypothesis.

With regard to presence or absence of periostitis, our study showed a statistically significant difference between the pre- and post-procedural MRIs ($p = 0.034$). Therefore, regression of periostitis may be used as an indicator of effective treatment in early follow-up period.

In evaluation of the presence or absence of joint effusion and synovitis on MRIs, we found no statistically significant difference between the pre- and post-procedural studies ($p = 0.625$ and $p = 1$ for effusion and synovitis, respectively). However, the extent of effusion and synovitis was markedly decreased in five patients after the procedure. Also, a negative correlation was found between the nidus-joint distance and the presence of effusion and synovitis ($p = 0.013$ and $p = 0.02$, for effusion and synovitis, respectively). These results of our study are in accordance with that of the previous studies suggesting that the production of high levels of prostaglandins from the nidus results in signs of joint effusion and/or synovitis when the nidus is located in close proximity to a joint.[10] Therefore, successful ablation of the nidus is expected to cause regression of the joint effusion/and or synovitis and this regression can be used as an indicator of successful treatment.

In three patients who demonstrated clinical and imaging findings of muscle atrophy before the procedure, the findings were almost completely regressed at 3rd month follow-up. However, this change didn't reach a statistical significance ($p = 0.25$).

Previous studies on MRI follow-up after RFTA of OO have reported that imaging appearances are well-correlated with the histopathologic changes occurring after the treatment.[6,10] On MR images Lee at al. described a target-like appearance of the ablated areas after RFTA treatment. According to their description, contrast-enhanced T1-weighted and T2-weighted images demonstrate 3 different zones after RFTA treatment: an inner non-enhanced hypointense zone (Z1), a well-enhancing, hyperintense rim (Z2) and a peripheral, less hyperintense zone of background tissue (Z3). In their study, the appearance of the treated areas was changed on follow-up MRIs.[6] The authors suggested that periodic monitoring of this specific MRI pattern might be used in treatment follow up. In follow-up examinations, showing the nidus of OO included within the area of Z1 was also reported to be a powerful indicator of treatment success.[6,14] In 11 out of 16 patients in our study (68.8%), this specific post-procedural MRI pattern was observed. In five patients (31.3%), the indicated pattern was absent. We didn't find a correlation between the presence of the described post-procedural MRI pattern and the VAS scores ($p = 1$), and no correlation was found between the timing of the post-procedural follow up MRI and the presence of the described MRI pattern ($p = 0.661$). While the study of Lee et al reported a significant relationship between the appearance of this MRI pattern and the timing of follow-up MR studies[6]; the results of our study did not support this relationship. We think that this difference in the results of the two study may be related to differences in nidi locations,

patient populations and the applied RFTA techniques. However, we believe that in cases that demonstrate a post-procedural target-like appearance on MRI, showing that the nidus is included within the area of Z1 may imply correct electrode positioning, and thus, may be used as an indicator of an effective treatment.

This study had certain limitations. Short-term clinical follow-up of the patients, small size of our patient population and the absence of a standardized RFTA treatment (e.g. in terms of duration of thermo-ablation and the use of variable temperatures) and the absence of any recurrent cases were the limitations of our study.

We found that successfully treated patients demonstrate a significant decrease in nidus size, nidus volume, nidus signal intensity and nidus contrast-enhancement in early follow-up period. Also, reactive periostitis and cortical thickening significantly regress after a successful treatment. Therefore, these findings, may be useful in predicting early treatment success in patients with OO. However, the nidus calcification, reactive cortical and/or intramedullary sclerosis, periosteal reaction and bone marrow and/or soft tissue edema didn't show significant differences between the pre- and post-procedural examinations and we think that these parameters are not reliable for predicting early treatment response. Overall, the value of conventional CT and MR findings was limited in our study and our results showed that these findings alone cannot be used with accuracy in early treatment follow up.

Conflict of interest

The authors declare that they have no conflict of interest.

References

1. Campanacci M. *Bone and Soft Tissue Tumors: Clinical Features, Imaging, Pathology and Treatment*. 2nd ed. Vienna: Austria: Springer Science & Business Media; 1999.
2. Pratali R, Zuiani G, Inada M, et al. Open resection of osteoid osteoma guided by a gamma-probe. *Int Orthop*. 2009;33:219–223.
3. Kransdorf MJ, Stull MA, Gilkey FW, Moser Jr RP. Osteoid osteoma. *Radiographics*. 1991;11:671–696.
4. Cohen MD, Harrington TM, Ginsburg WW. Osteoid osteoma: 95 cases and a review of the literature. *Semin Arthritis Rheum*. 1983;12:265–281.
5. Clark T, Sabharwal T. *Interventional Radiology Techniques in Ablation*. 1st ed. London: England: Springer Science & Business Media; 2013.
6. Lee MH, Ahn JM, Chung HW, et al. Osteoid osteoma treated with percutaneous radiofrequency ablation: MR imaging follow-up. *Eur J Radiol*. 2007;64:309–314.
7. Ronkainen J, Blanco Sequeiros R, Tervonen O. Cost comparison of low-field (0.23 T) MRI-guided laser ablation and surgery in the treatment of osteoid osteoma. *Eur Radiol*. 2006;16:2858–2865.
8. Teixeira PA, Chanson A, Beaumont M, et al. Dynamic MR imaging of osteoid osteomas: correlation of semiquantitative and quantitative perfusion parameters with patient symptoms and treatment outcome. *Eur Radiol*. 2013;23:2602–2611.
9. Liu PT, Chivers FS, Roberts CC, Schultz CJ, Beauchamp CP. Imaging of osteoid osteoma with dynamic gadolinium-enhanced MR imaging. *Radiology*. 2003;227:691–700.
10. Vanderschueren GM, Taminiau AH, Obermann WR, van den Berg-Huysmans AA, Bloem JL, van Erkel AR. The healing pattern of osteoid osteomas on computed tomography and magnetic resonance imaging after thermocoagulation. *Skelet Radiol*. 2007;36:813–821.
11. Martel J, Bueno A, Ortiz E. Percutaneous radiofrequency treatment of osteoid osteoma using cool-tip electrodes. *Eur J Radiol*. 2005;56:403–408.
12. Rehnitz C, Sprengel SD, Lehner B, et al. CT-guided radiofrequency ablation of osteoid osteoma: correlation of clinical outcome and imaging features. *Diagn Interv Radiol*. 2013;19:330–339.
13. Kawaguchi Y, Sato C, Hasegawa T, Oka S, Kuwahara H, Norimatsu H. Intra-articular osteoid osteoma associated with synovitis: a possible role of cyclooxygenase-2 expression by osteoblasts in the nidus. *Mod Pathol*. 2000;13:1086–1091.
14. Lee JM, Choi SH, Park HS, et al. Radiofrequency thermal ablation in canine femur: evaluation of coagulation necrosis reproducibility and MRI-histopathologic correlation. *Am J Roentgenol*. 2005;185:661–667.